Mechanisms of catalysis and allosteric regulation of yeast chorismate mutase from crystal structures

Norbert Sträter[1,2], Georg Schnappauf[3], Gerhard Braus[3] and William N Lipscomb[1]*

Background: Chorismate mutase (CM) catalyzes the Claisen rearrangement of chorismate to prephenate, notably the only known enzymatically catalyzed pericyclic reaction in primary metabolism. Structures of the enzyme in complex with an *endo*-oxabicyclic transition state analogue inhibitor, previously determined for *Bacillus subtilis* and *Escherichia coli* CM, provide structural insight into the enzyme mechanism. In contrast to these bacterial CMs, yeast CM is allosterically regulated in two ways: activation by tryptophan and inhibition by tyrosine. Yeast CM exists in two allosteric states, R (active) and T (inactive).

Results: We have determined crystal structures of wild-type yeast CM co-crystallized with tryptophan and an *endo*-oxabicyclic transition state analogue inhibitor, of wild-type yeast CM co-crystallized with tyrosine and the *endo*-oxabicyclic transition state analogue inhibitor and of the Thr226→Ser mutant of yeast CM in complex with tryptophan. Binding of the transition state analogue inhibitor to CM keeps the enzyme in a 'super R' state, even if the inhibitory effector tyrosine is bound to the regulatory site.

Conclusions: The *endo*-oxabicyclic inhibitor binds to yeast CM in a similar way as it does to the distantly related CM from *E. coli*. The inhibitor-binding mode supports a mechanism by which polar sidechains of the enzyme bind the substrate in the pseudo-diaxial conformation, which is required for catalytic turnover. A lysine and a protonated glutamate sidechain have a critical role in the stabilization of the transition state of the pericyclic reaction. The allosteric transition from T→R state is accompanied by a 15° rotation of one of the two subunits relative to the other (where 0° rotation defines the T state). This rotation causes conformational changes at the dimer interface which are transmitted to the active site. An allosteric pathway is proposed to include residues Phe28, Asp24 and Glu23, which move toward the active-site cavity in the T state. In the presence of the transition-state analogue a super R state is formed, which is characterised by a 22° rotation of one subunit relative to the other.

Addresses: [1]Department of Chemistry and Chemical Biology, Harvard University, 12 Oxford Street, Cambridge, MA 02138, USA, [2]Institut für Kristallographie, Freie Universität Berlin, Takustrasse 6, D-14195 Berlin, Germany and [3]Institut für Mikrobiologie und Genetik, Georg-August-Universität, Grisebachstrasse 8, D-37077 Göttingen, Germany.

*Corresponding author.
E-mail: Lipscomb@chemistry.harvard.edu

Key words: allosterism, Claisen rearrangement, pericyclic reaction, transition state analogue inhibitor, X-ray crystallography

Received: **18 July 1997**
Revisions requested: **14 August 1997**
Revisions received: **22 September 1997**
Accepted: **22 September 1997**

Structure 15 November 1997, **5**:1437–1452
http://biomednet.com/elecref/0969212600501437

 ISSN 0969-2126

Introduction

Chorismic acid lies at the first branch point of the biosynthetic pathway of the aromatic amino acids tryptophan, phenylalanine and tyrosine (Figure 1; [1,2]). In one branch, which leads to the production of tryptophan, chorismate is the substrate of the heterodimeric enzyme anthranilate synthase. In the other branch, chorismate mutase (CM, chorismate pyruvatemutase; E.C. 5.4.99.5) catalyzes the intramolecular rearrangement of chorismate to prephenate, the first committed step in the synthesis of tyrosine and phenylalanine. In the yeast *Saccharomyces cerevisiae*, the activity of CM is modulated by a ~tenfold activation by tryptophan and a ~tenfold feedback inhibition by tyrosine [3]. The 100-fold modulation of the enzyme activity by these two amino acids controls the flux of chorismic acid into the phenylalanine/tyrosine-biosynthetic branch in relation to the tryptophan branch, where anthranilate synthase competes with chorismate mutase for the common substrate. Activation and inhibition are mainly caused by a change in K_m along with relatively small changes in k_{cat}. The active R form of CM has a pH optimum of 6.5, whereas optimum activity is seen at pH 5.0 in the inactive T form.

Yeast CM (YCM) is a homodimer of two 30 kDa polypeptides. As a relatively small protein in the allosteric family, YCM provides an ideal system for exploring the detailed mechanisms of allosteric regulation. Crystal structures of YCM have been determined for the Thr226→Ile mutant [4], which is trapped in the active R state, and for the

Figure 1

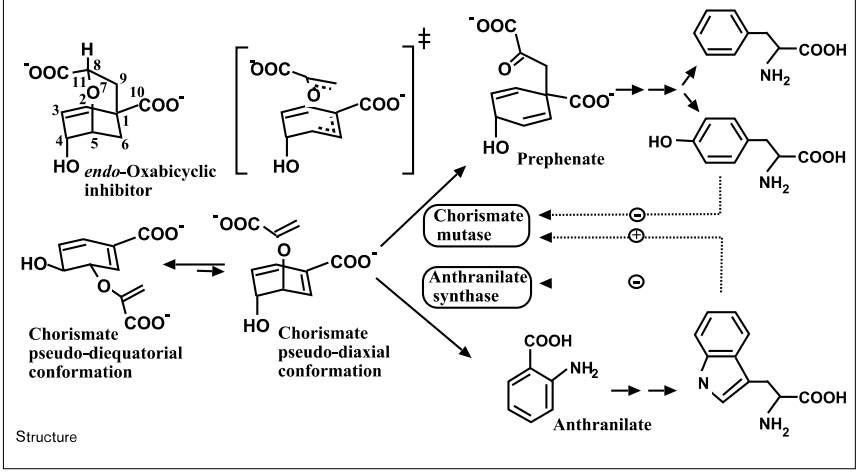

Conversion of chorismate to prephenate by chorismate mutase in relation to the biosynthesis of aromatic amino acids. Also shown are two conformers of chorismate, the transition state of the pericyclic reaction and an *endo*-oxabicyclic transition state analogue inhibitor.

tyrosine-bound wild-type enzyme in the T state [5]. A comparison of these structures showed that the allosteric transition includes a 15° rotation of one of the two catalytic domains relative to the other. It was also demonstrated that both allosteric effectors, tryptophan and tyrosine, bind to the same binding site at the dimer interface. Although differences were apparent between the active sites in the R state and in the T state structures, it was yet difficult to relate these changes to the modulation of enzyme activity because detailed structural information on the binding mode of the substrate or transition state was not available.

The catalysis of a pericyclic reaction by chorismate mutase has stimulated many biochemical, computational and structural studies (reviewed in [6]). Molecular orbital calculations [7,8] and studies of isotope effects using labeled substrate [9,10] indicate that, in both the uncatalyzed and catalyzed reactions, the rearrangement of chorismate to prephenate proceeds through a transition state with chair-like geometry. In solution, 10–20% of chorismate exists in the energetically less favored pseudo-diaxial form in dynamic equilibrium with the pseudo-diequatorial form (Figure 1; [11]). It has thus been proposed that the reaction is accelerated by binding of the active diaxial conformer to the enzyme [12]. Catalysis of the [3,3]-sigmatropic rearrangement might proceed by attack of an enzyme nucleophile at C5 leading to the formation of an intermediate [10], or in a concerted but perhaps asynchronous pericyclic process like the uncatalyzed reaction [13]. Rate enhancement of the pericyclic reaction was proposed to be achieved by electrostatic stabilization of the transition state [13], which might have a dipolar character after heterolytic cleavage of the C–O bond. Strong binding of an *endo*-oxabicyclic transition-state analog [14] suggests that the enzyme-catalyzed reaction may proceed via a similar transition state.

Detailed structural insight into the mechanism of these enzymes was first obtained by structure determinations of *Bacillus subtilis* CM in the unligated form, in complex with the product prephenate and in complex with the *endo*-oxabicyclic transition-state analog (Figure 1; [15,16]). Later, the X-ray structure of YCM was determined for the activated R state [4]. More recently, the structure of the CM domain of the P protein from *Escherichia coli* was determined with the transition state analogue inhibitor bound to the active site, and it was found to be related to YCM [17]. On the basis of this relationship to *E. coli* CM, the active site in YCM could be located [18]. The active-site cavity in *E. coli* CM is surrounded by a four-helix bundle which can be superimposed onto a similar helix bundle in YCM, yielding 22% sequence identity of 94 residues. Mutational analysis of all critical active-site residues in YCM confirmed the proposed location of the active site and quantified their contribution to catalysis [19].

The *endo*-oxabicyclic transition-state analogue has also been used to generate antibodies that have CM activity. The crystal structure of one of these catalytic antibodies (1F7), which achieves a 250-fold rate enhancement over the uncatalyzed reaction, is available in complex with the *endo*-oxabicyclic inhibitor [20]. The most active abzyme, 11F1–2E11, gave a 10^4-fold rate enhancement compared to a ~10^6-fold rate acceleration by the wild-type enzymes [21]. The known CM structures, except that of YCM, have been discussed previously [22].

Here, we present two crystal structures of YCM in complex with an *endo*-oxabicyclic transition-state analogue and with either the allosteric activator tryptophan (ITRP) or the allosteric inhibitor tyrosine (ITYR). Also, a high resolution crystal structure of the tryptophan-bound R form of the Thr226→Ser mutant of YCM (STRP) is presented in space

group C2. The three new structures are compared with the structures of wild-type YCM in the T state, the Thr226→Ile mutant of YCM in the R state and the structures of *B. subtilis* and *E. coli* CM. Together, these structures support a mechanism by which polar sidechains of the enzyme bind the substrate in the pseudo-diaxial conformation, which is required for catalytic turnover via a pericyclic reaction pathway. A lysine and a protonated glutamate sidechain have a critical role in the stabilization of the transition state of the pericyclic reaction. An analysis of the structures in different allosteric states shows that the allosteric transition is accompanied by a rotation of the two subunits relative to each other. This rotation causes conformational changes at the dimer interface where Phe28 and Tyr212 interact. A detailed allosteric pathway is proposed to include these sidechains as well as Asp24, Lys208, Arg204, and Glu23, which transmit the allosteric signal to the active site.

Results

Enzyme structure

YCM is essentially an all-helix structure; each monomer has 12 helices, of which four (H1, H3, H5 and H6) contain only one turn. The longer helices are shown with labels in Figure 2. H8, the longest helix, contains 32 residues and spans the whole monomer; it also connects the catalytic site with the regulatory site. The active site is located between helices H2, H8, H11 and H12, which together with helices H7 H9, and H10 form the catalytic domain. Helix H4 and loops L50s (residues 44–58) and L80s (residues 79–107) are part of the regulatory domain. The two allosteric effectors bind to the regulatory site at the dimer interface. On one side this site has helix H8 of one monomer, whereas on the other side the second monomer supplies the 80s loop and helices H4 and H5. Dimeric YCM has dimensions of $90 \times 55 \times 55$ Å. A strong hydrophobic association between the monomers at the dimer interface is mediated by helices H2, H4, H8 and H11. Also the loops L80s and L50s of the regulatory domain participate in inter-subunit interactions.

To facilitate the following description of our results and discussion, which depends on comparisons of different structures, Table 1 summarizes the main characteristics of the structures discussed in this article and gives abbreviations which are used in the following text.

Figure 2

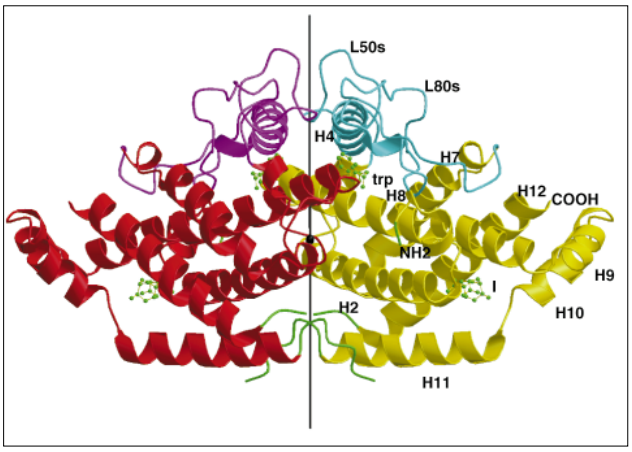

Structure of the YCM dimer. The catalytic domains are colored yellow and red, the regulatory domains cyan and purple. Shown in green are the *endo*-oxabicyclic inhibitor (**I**) bound to the active sites and tryptophan bound at the regulatory sites. The view is along the allosteric rotation axis perpendicular to the dimer axis (both axes shown in black). The rotation along the allosteric axis (represented by a filled circle) from the T to the R state is such that the catalytic domain of the left subunit rotates clockwise and that of the right subunit counter-clockwise (see also Figure 9).

The active site and inhibitor binding

Binding of the *endo*-oxabicyclic inhibitor to the presumed [18] active-site pocket was clearly demonstrated by the electron density maps (Figure 3a). Due to the compact shape of the bicyclic structure of the inhibitor, the electron density had roughly a spherical shape at the relatively low resolution of the data. The lobes caused by the inhibitor's carboxylate and hydroxyl groups, however, were clearly visible even before the inhibitor was introduced into the model and helped to determine the orientation of the inhibitor. This binding mode of the

Table 1

Characteristics of the structures discussed in this article.

Structure	Protein	Ligands	State	Space group	Resolution (Å)	pH	PDB code	Reference
TRP	T226I	tryptophan	R	P61	2.2	8.0	1csm	[4]
TYR	wild type	tyrosine	T	$P4_32_12$	2.8	5.0	2csm	[5]
ITRP	wild type	inhibitor + tryptophan	super R	R32	3.0	8.0	3csm	this study
ITYR	wild type	inhibitor + tyrosine	super R	R32	2.8	9.0	4csm	this study
STRP	T226S	tryptophan	R	C2	2.0	5.0	5csm	this study

Figure 3

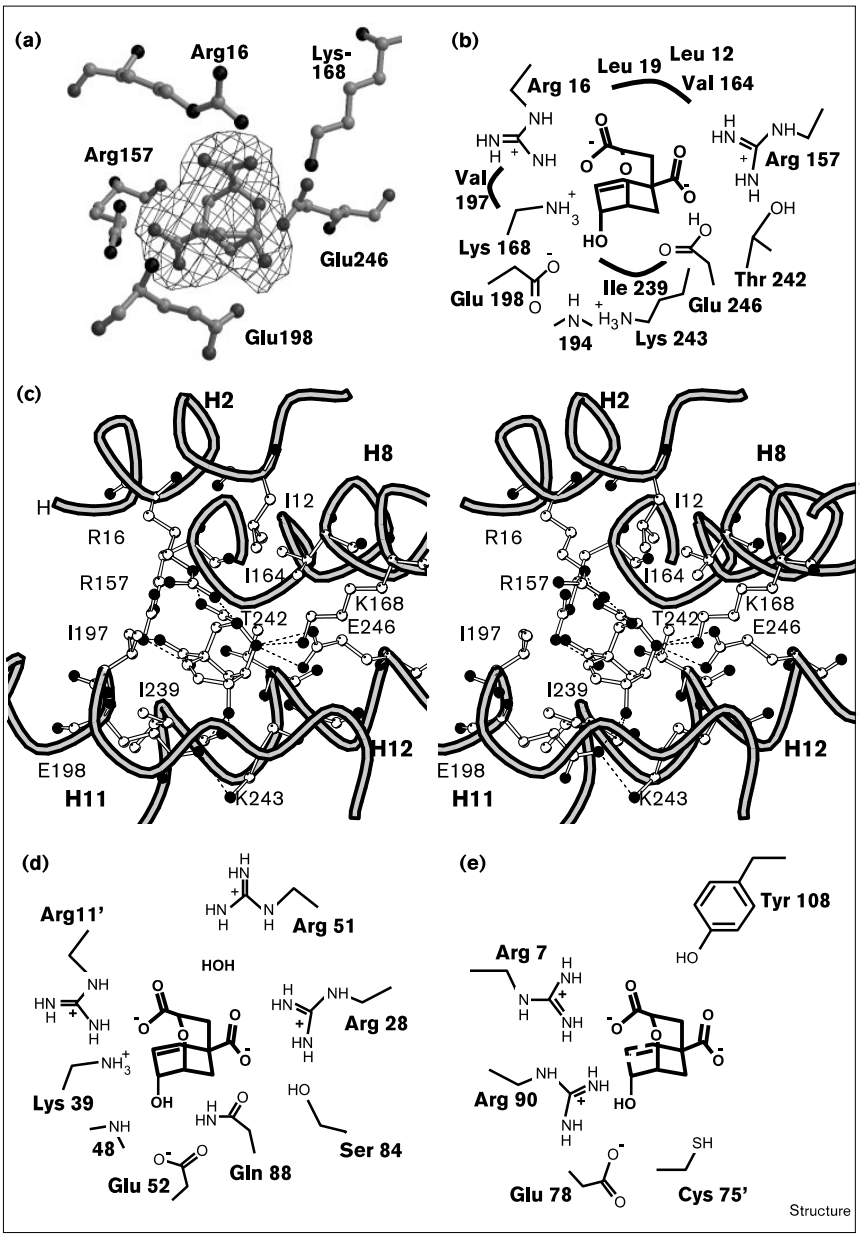

Binding mode of the *endo*-oxabicyclic inhibitor to the active site. **(a)** 2.8 Å $|F_o-F_c|$ difference electron density of the inhibitor in ITYR. Also shown are the sidechains of those residues which have polar interactions with the inhibitor. **(b)** Scheme of interactions between the inhibitor and active site residues of YCM. **(c)** Stereo view of the binding mode of the inhibitor to the active site in ITRP. **(d,e)** Binding of the *endo*-oxabicyclic inhibitor to *E. coli* CM (d) and to *B. subtilis* CM (e). All proton positions in (b) are inferred. Pending identification of pK_as, mechanisms are possible in which the carboxylate group of Glu246 is ionized.

transition-state analogue (Figure 3) confirms the model for inhibitor binding, which was proposed on the basis of the homology of YCM to *E. coli* CM [18].

Interestingly, the structures of the active sites are practically identical in ITRP (YCM in complex with the inhibitor and tryptophan) and ITYR (bound inhibitor and tyrosine). All polar sidechains of the active sites have very similar conformations and positions. Only the hydrophobic sidechains of Ile239 and Ile192 have been refined to different conformations of the χ^1 and χ^2 torsion angles, respectively; however, these sidechains still have similar positions.

The guanidinium groups of Arg16 and Arg157 bind the two carboxylate groups of the inhibitor, whereas its hydroxyl group is hydrogen bonded to the sidechain of Glu198 and to the backbone NH group of Asn194 (Figure 3). Lys168 and Glu246 are in hydrogen-bonding distance to the ether oxygen O7 of the inhibitor. In addition, hydrophobic contacts with Leu19, Leu12, Val164, Val197, Ile239 and the sidechain carbons of Lys243 contribute to inhibitor binding.

Figure 4

Superposition of the five YCM structures in different allosteric states. Superimposed on the basis of the Cα atoms of monomer A (upper half) are TYR (black), TRP (blue), STRP (green), ITRP (red) and ITYR (yellow). Monomer B is shown in lower half of figure; see Table 1 for descriptions of different YCM structures. Also shown is tryptophan bound to the allosteric site.

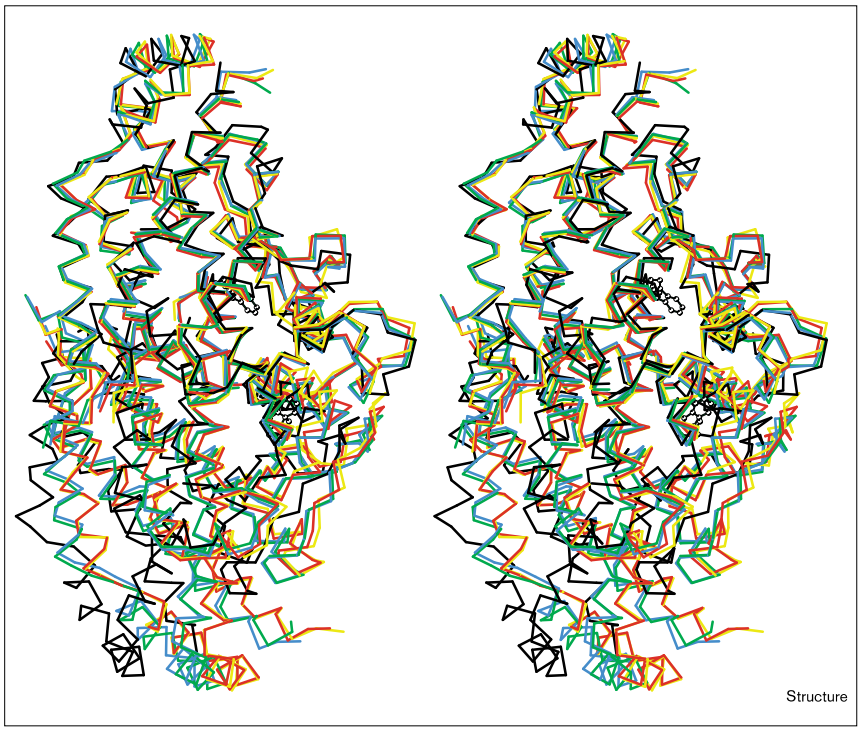

All active-site sidechains are well defined in the electron-density maps (data not shown). The close distance of 2.8 Å between the carboxylate group of Glu246 and the inhibitor's ether oxygen suggests that this sidechain is protonated, despite the relatively high pH value at which the crystals were obtained (pH 8–9). Protonation at high pH values is supported by the pH rate profile for the R-state enzyme, which has maximum activity at pH 7.0 and shows around 30% activity at pH 9.0 [3]. In the tryptophan-activated enzyme (ITRP), the distances from the inhibitor's ether oxygen atom to Oε1 and Oε2 of Glu246 are both relatively long (3.1 and 3.2 Å, respectively). At the resolution of the present study, however, the sidechain positions are not that accurately defined and it is possible that one oxygen, which may be protonated, is actually closer to the ether oxygen of the inhibitor, similar to the situation in ITYR (distances of 3.3 and 2.8 Å between the ether oxygen of the inhibitor and Oε1 and Oε2 of Glu246).

Superposition of the different allosteric states

Figure 4 shows a superposition of the five structures that have been determined for YCM. Atoms of only one monomer (shown in the upper half of Figure 4) were used to calculate the matrix for this superposition. As outlined in the introduction, the allosteric transition is accompanied by a rotation of the two subunits relative to each other. Thus, differences seen in the other monomer in Figure 4 (lower half) are mainly due to different allosteric states. Not surprisingly, the T-state structure TYR (black) is most different from all other structures. The structures of STRP (green), the Thr226→Ser mutant in complex with tryptophan, and TRP (blue), the previously determined R-state structure, are similar to each other. Interestingly, ITRP (red) as well as ITYR (yellow) are even more different from the T-state than the R-state structures (TRP and STRP). Not only are the structures of the active site in ITRP and ITYR very similar (see previous section), the catalytic domains of these two structures also superimpose closely (Figure 4). After the two structures have been superimposed on the basis of the catalytic domain of one subunit, the catalytic domain of the other subunit is aligned as well. This surprising result demonstrates that both structures are in the same allosteric R-like state even though tyrosine (an allosteric inhibitor) is bound to ITYR. The active-site inhibitor keeps the enzyme tightly locked in a state which is in the direction of the T→R transition even beyond TRP, the tryptophan-activated R state. This novel structure may thus be designated a 'super R' state. The only significant differences between ITRP and ITYR are seen in the regulatory domain, which has moved toward the T state in ITYR, but is not identical to it (see below).

The structural differences related to the allosteric transition may be quantified by using all atoms of the dimer in

a superposition to calculate a root mean square (rms) deviation. TYR differs from ITRP as well as ITYR by the maximum value of 3.2 Å. STRP and TRP, which have rms differences from TYR of 2.5 and 2.4 Å, respectively, are somewhat closer to the T state. ITYR and ITRP differ by 0.7 Å, STRP and TRP by 0.5 Å. Another way to quantify the differences between the allosteric states is using the angle by which the monomers rotate relative to each other around the allosteric rotation axis in the T→R transition. This rotation angle relative to TYR is 22.0° and 21.7° for the super R state structures ITRP and ITYR, whereas rotations relative to TYR of 14.8° and 16.2° characterize the R state structures TRP and STRP, respectively. The axis of rotation is perpendicular to the dimer axis (twofold rotation axis relating the two subunits) as shown in Figure 2. The direction of the rotation is such that if the right monomer in Figure 2 (shown in yellow) is fixed, the other monomer rotates clockwise in the T→R transition.

The allosteric transition is also accompanied by smaller changes within the catalytic domain, which account for the lower or impaired activity of the T state. The rms differences between the catalytic domains (calculated after superposition of these domains) correlate with those deviations between the dimers — the structures which are most different along the allosteric transition also show more changes within their catalytic domains. Again, the catalytic domain of the T-state structure TYR is more different from ITRP and ITYR (both having an rms deviation of 1.4 Å) than from R-state structures TRP and STRP (1.1 and 1.2 Å, respectively).

The regulatory site

The 2.0 Å structure of STRP provides a detailed picture of the structure of the regulatory site in the R state. Tryptophan has four direct polar interactions with residues of helix H8 (Figure 5a; Table 2), but it has only hydrophobic contacts to H4/H5 of the other subunit, mainly between its six-membered ring and Ile74. In addition, tryptophan is hydrogen bonded to five water molecules: the carboxylate group interacts with three water molecules, the amino group with one water molecule and the sidechain nitrogen with another (for clarity water molecules are not shown in Figure 5). The binding mode of tryptophan and the structure of the regulatory site show no significant differences between ITRP, TRP and STRP.

A superposition of ITYR with T- and R-state structures showed that ITYR is in the active R state (see above). Difference electron-density maps, however, clearly demonstrated that the allosteric inhibitor tyrosine, which was present in the crystallization buffer at a concentration of 2 mM, is bound to the regulatory site (Figure 5b). The density of the effector was well defined and the sidechain had the shape of the phenol group of tyrosine, but not that of the larger tryptophan sidechain. As a result of the binding of the allosteric inhibitor, tyrosine, to the R-state structure of the enzyme, the regulatory site in ITYR has a structure which is between that in the R state and that in the T state (Figure 5; Table 2). Although Arg75 and Arg76 have polar interactions with the tyrosine ligand which are characteristic of the T state [5], a superposition of the regulatory sites in TYR and ITYR shows differences in mainchain and sidechain positions of the protein and the inhibitor (Figure 4d). The sidechain of Arg75, in particular, is not properly positioned to have as favorable hydrogen-bonding interactions as seen in the T state. Also, the guanidinium group of Arg76 in ITYR is (despite a similar hydrogen-bonding distance) not as well oriented for a hydrogen-bonding interaction with the allosteric inhibitor as it is in TYR (Figure 5d).

A superposition of the regulatory sites in ITYR and ITRP demonstrates significant differences in this region (Figure 5c). The hydrophobic contact between the six-membered ring of tryptophan and Ile74 pushes the 80s loop apart from helix H8 of the other subunit. In ITYR, this loop is closer to the effector and Arg75 interacts with the carboxylate group of tyrosine. Maximum differences around 2–3 Å are present in the position of some residues of the 80s loop between ITYR and ITRP. Thus, there are differences in the region around the regulatory site in ITYR from that of TYR as well as ITRP.

The 220s loop and amino acid 226

Mutations of Thr226 significantly influence the allosteric behavior of YCM. Various replacements of Thr226 have been characterized kinetically, showing that these mutations shift the enzyme toward the R state to different degrees [23]. The Thr226→Ile mutant, for which the first structure of the enzyme was determined (TRP; [4]), is locked in the R state. In the tyrosine-bound T-state structure of wild-type YCM (TYR), the sidechain of Thr226 may be hydrogen bonded to either the carboxylate group of Glu228 or to the backbone carbonyl group of Arg224 via a water molecule [5]. Amino acid 226 is at the connection between helix H12 and the 220s loop, which is largely disordered in all four crystal forms of YCM. The disordered region comprises residues 218–221 in TRP, ITRP and ITYR, 215–223 in TYR and 218–223 in STRP. Those residues of this loop (212–226) that are visible in the electron-density maps, however, indicate that the position of this loop changes significantly during the allosteric transition.

The allosteric behavior of the Thr226→Ser mutant, the structure of which is described here, is also shifted toward the R state, although less than in other Thr226 mutants [23]. The hydroxyl group of the sidechain of Ser226 in STRP is hydrogen bonded to the backbone

Figure 5

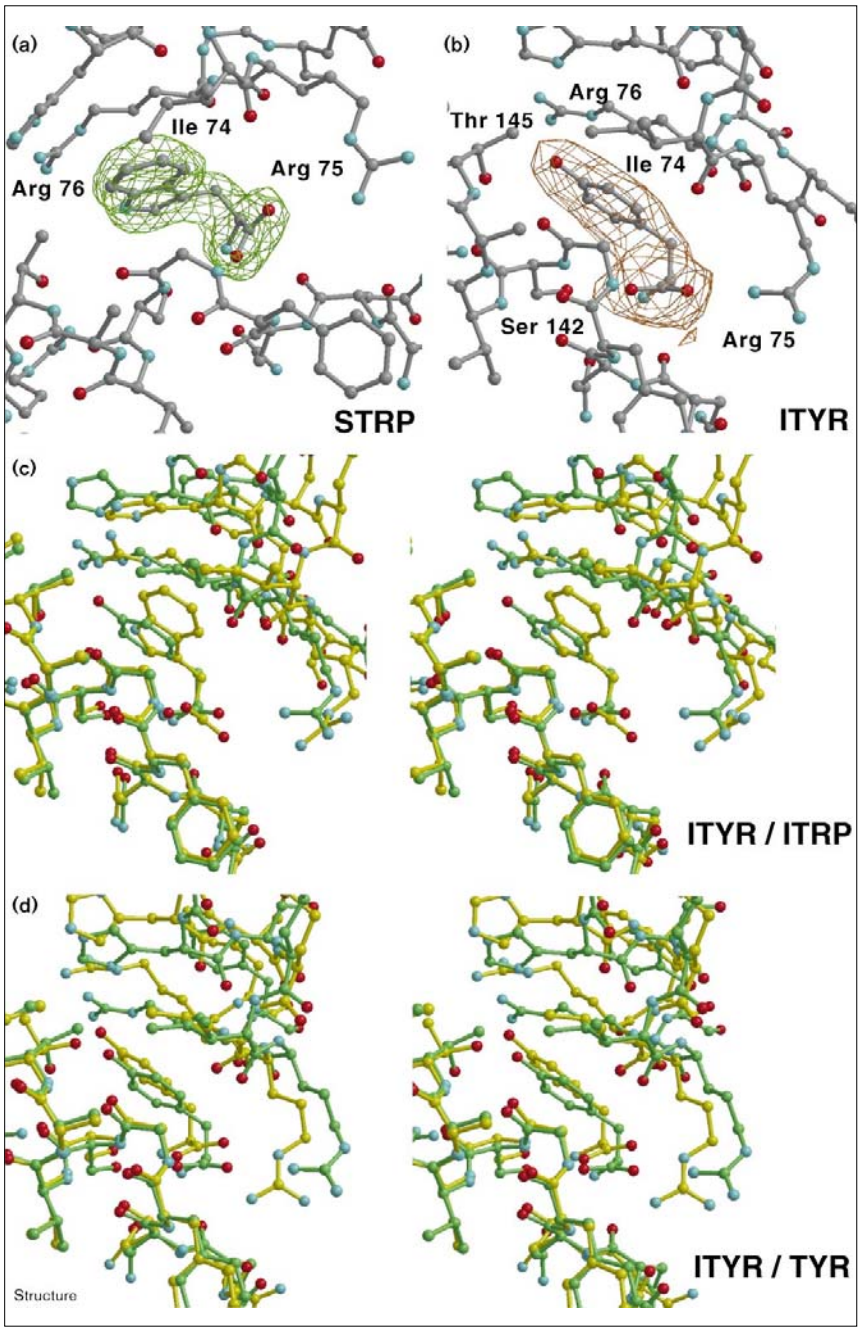

Structure of the regulatory binding site. **(a)** F_o–F_c difference electron density map of tryptophan bound to the regulatory site in STRP. **(b)** F_o–F_c difference electron density map of tyrosine bound to ITYR. **(c)** Superposition of ITYR (green) and ITRP (yellow) based on the Cα atoms of the catalytic domain (see Materials and methods). **(d)** Superposition of ITYR (green) and TYR (yellow) based on the Cα atoms of residues 133–152. Nitrogen atoms are colored blue and oxygens red.

NH group of Glu228. Although structures of two mutants carrying amino acid replacements at position 226 are known in addition to the wild-type enzyme structure, it remains difficult to explain the role of this residue and the 220s loop in the allosteric transition. The most likely explanation is that if large sidechains are present at position 226, the 220s loop is sterically prevented from gaining a conformation which is necessary for the formation of the T state. This suggestion, however, does not account for the stronger tyrosine inhibition of the wild-type enzyme than that of the Thr226→Ser mutant. Mutations or deletions of the other residues of the 220s loop might probe the significance of this partially disordered loop in the allosteric transition. Further indication of the importance of this loop arises from the analysis of a proposed allosteric pathway (see below).

Table 2

Selected distances (Å) between tyrosine or tryptophan and residues of the regulatory site.

Ligand atom	Protein atom	ITYR*	TYR	ITRP	STRP	TRP*
N	O, AsnB138	2.8	3.8	3.4	3.3	3.3
	Oδ1, AsnB139	3.3	3.5	3.3	3.4	3.2
	Oγ, SerB142	3.3	2.4	2.9	3.0	2.8
O	N, GlyB141	2.7	2.8	2.7	2.9	3.0
	N, SerB142	2.9	2.8	3.6	3.1	3.0
O′	Nη, ArgA75	4.2	3.2	4.9	5.0	5.0
	Nε, ArgA75	5.6	2.7	5.1	5.0	5.0
OH	Nε, ArgA76	3.2	3.3	–	–	–
	Oγ1, ThrB145	3.2	3.1	–	–	–

*Distances have been averaged over the two independently refined monomers in the asymmetric unit.

Discussion

Comparison to other chorismate mutases

As a result of the conserved active-site pockets, the binding mode of the *endo*-oxabicyclic inhibitor in YCM is very similar to that in *E. coli* CM [17] (Figures 3b, 3d and 6a). The major difference between the two enzymes is the presence of Glu246 in the active site of YCM, whereas *E. coli* CM displays a corresponding glutamine (Gln88). Gln88 is hydrogen bonded to the ether oxygen of the inhibitor and obviously has an important role in the enzyme mechanism. Another difference is that the sidechain of YCM residue Thr242 was refined to a conformation in which the hydroxyl group is not hydrogen bonded to the C10 carboxyl group of the inhibitor, contrary to what might be expected from an analogous interaction of Ser84 of *E. coli* CM with the inhibitor (Figure 3d). Thr242 instead interacts with the backbone carbonyl group of Val238; however, Thr242 is essential for YCM activity [19].

In *B. subtilis* CM, the inhibitor has similar polar interactions with the enzyme [15,16]. Here, the guanidinium group of Arg90 is hydrogen bonded to the ether O7 oxygen atom of the inhibitor (Figure 3e). In *B. subtilis* CM, the inhibitor interacts through one of its carboxylate groups with Arg7 and its hydroxyl group with Glu78, similar to interactions in YCM and *E. coli* CM; however, the polar interactions between the second carboxylate group of the inhibitor and the protein are absent in *B. subtilis* CM. The active site of *B. subtilis* CM is somewhat open and more solvent accessible than the more buried catalytic pockets in YCM and *E. coli* CM.

Evolutionary relationship between *E. coli* CM and YCM

It has been noted earlier that the dimer of *E. coli* CM can be superimposed onto a monomer of YCM, indicating a common evolutionary origin of the two enzymes. [17,18]. Here, we discuss the relationship between the two CMs in the light of more recent data on the allosteric transition. The CM domain (N-terminal 109 residues) of the *E. coli* P protein consists of three helices H1–H3. Two fragments of the *E. coli* CM domain dimerize such that two active sites are formed between a four-helix bundle of H1, H2, H3 and H1′ (where H′ represents helices from the adjacent monomer; Figure 6). In YCM, helices H2, H4, H7, H8, H11 and H12 correspond to H1′, H2′, H3′, H1, H2 and H3 in *E. coli* CM. Thus, in YCM helices H2, H4, and H7 are related by a common origin to helices H8, H11 and H12, indicating a gene duplication event in the evolution of YCM.

A superposition of YCM and *E. coli* CM shows that the helices forming the active site in YCM are most conserved between the two enzymes (Figure 6a). Also, the position and binding mode of the *endo*-oxabicyclic inhibitor are very similar. Thus, this region of the yeast enzyme corresponds largely to one monomer of *E. coli* CM (Figure 6a; red) and the structures superimpose well. A region composed of 94 residues has an rms difference of 1.06 Å between the two CMs and shows 22% sequence identity [18]. The main difference between the enzymes in this region is the presence of the partially disordered 220s loop in YCM, which probably plays a role in the allosteric regulation. The other monomer of the bacterial CM has become more diverged in YCM. The region around the second active site of *E. coli* CM is significantly reduced in YCM. The loop between helices H7 and H8, the loop which forms the connection between the two gene-duplicated pre-domains in YCM, and part of the 50s loop are close to the location of the 'former' second active site. Helix H2′ of *E. coli* CM and H4 in YCM have diverged significantly such that H4 forms the regulatory domain in

Figure 6

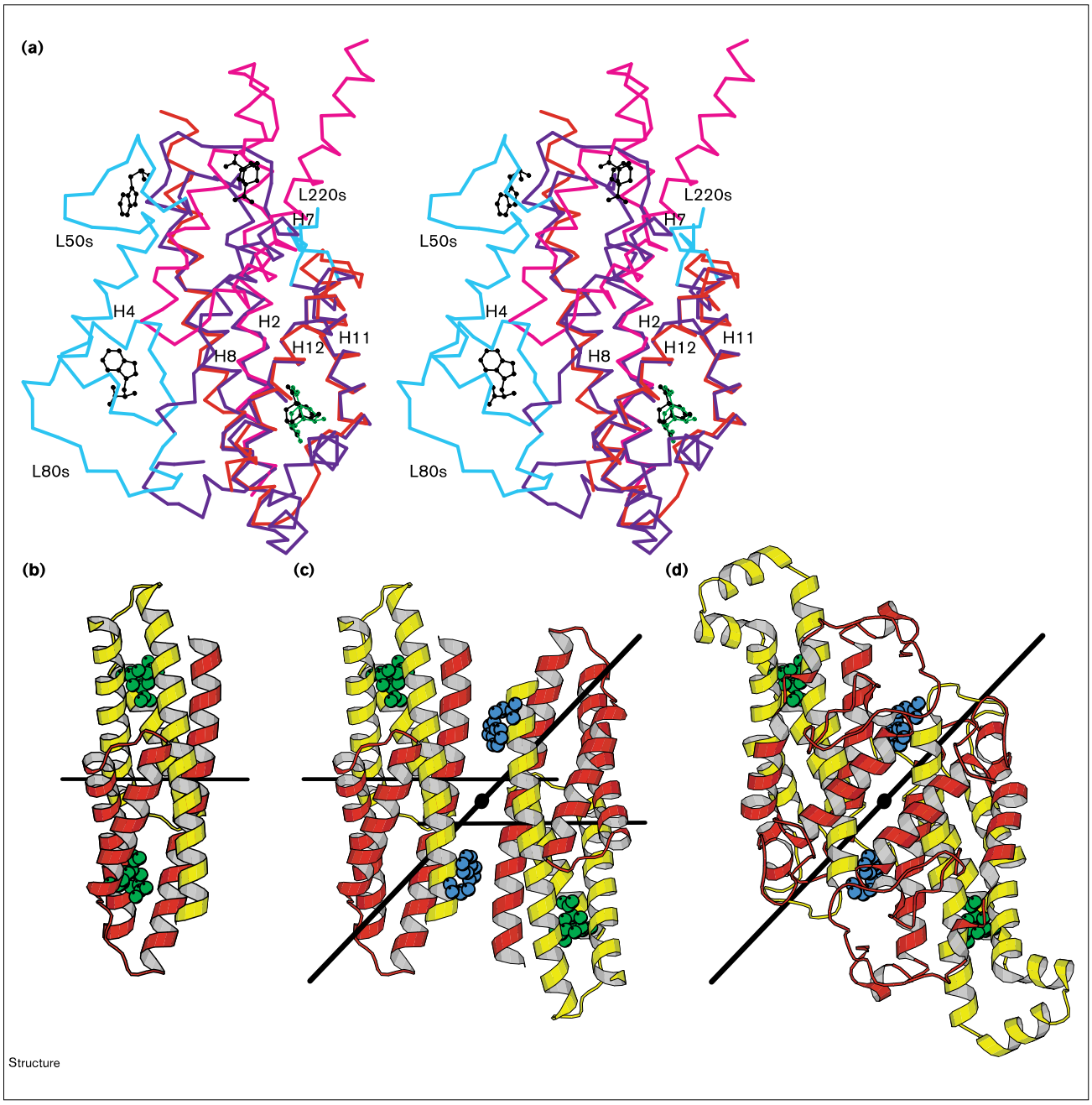

Evolutionary relationship between *E. coli* CM and YCM. **(a)** Superposition of the dimer of *E. coli* CM onto the monomer of YCM (see materials and methods). The two monomers of *E. coli* CM are colored red and magenta. The catalytic and regulatory domains of YCM are shown in blue and cyan, respectively. Also shown are tryptophan (black) bound to the two regulatory binding sites in YCM, the *endo*-oxabicyclic inhibitor bound to YCM in green and bound to the two active sites of the *E. coli* CM dimer in black. **(b)** *E. coli* CM dimer with the *endo*-oxabicyclic inhibitor (in green) bound to both active sites. The twofold rotation axis relating the two monomers (yellow and red) is shown as a black line. **(c)** Constructed tetrameric molecule of two *E. coli* CM dimers derived from a superposition onto the YCM dimer (not shown). Only those models for the inhibitor which are bound to the conserved active sites between *E. coli* CM and YCM are shown in green. The binding sites for the allosteric effectors in YCM are marked by models for tryptophan shown in blue. The local dimer axes of the *E. coli* dimers are shown as short black lines, the allosteric rotation axis of YCM is marked as a long black line. The view is along a twofold rotation axis relating the two dimers of the constructed molecule. **(d)** YCM dimer viewed along the dimer axis in the same orientation as the constructed tetramer. The two halves of each monomer are colored red or yellow, based on the corresponding monomers of the *E. coli* dimer.

YCM (Figure 6a; cyan). In addition, the long 50s and 80s loops, which also belong to the regulatory domain have formed, flanking H4.

E. coli CM has a much simpler fold and structure than YCM and also lacks allosteric regulation, so it may be assumed that the evolutionary precursor of the two enzymes was similar to *E. coli* CM. From this ancestral protein, which may also have been a dimer like *E. coli* CM, YCM has evolved by gene duplication, allowing for the formation of the regulatory domain, and by dimerization (or by tetramerization if the oligomerization event preceded the gene duplication). Figures 6b–d illustrate the formal construction of a tetrameric molecule from the *E. coli* CM dimer, if each dimer is superimposed onto one monomer of YCM. The tetramer has a symmetry that is related to D_2 (or *222*, having three perpendicular twofold axes). The two twofold dimer axes of each *E. coli* dimer are not aligned, but are parallel at a distance of 7 Å in the projection shown in Figures 6b–d. The allosteric rotation axis, around which the catalytic subunits rotate in the T→R transition, forms an angle of 46° to these local twofold axes of each *E. coli* dimer. The two parallel dimer axes are approximately in the same plane perpendicular to the YCM dimer axis if the tetramer is constructed for the T state structure, whereas the ~20° rotation around the allosteric axis tilts the two axes by 10° in opposite directions relative to the paper plane in the R state tetramer. For orientation, the binding sites for the allosteric effectors at the YCM dimer interface and for the active sites are also marked in the constructed tetramer in Figure 6b. The long helices H1 and H1′ of each *E. coli* CM dimer form the four-helix bundle at the dimer interface of YCM (two H2 and two H8). A comparison to the structure of the YCM dimer also demonstrates that mostly one half (red-colored) of each monomer in YCM have changed to form the regulatory subunit at the dimer interface.

Enzyme mechanism

Structures of YCM in complex with the *endo*-oxabicyclic inhibitor showed similar binding of this transition-state analogue to the active site of YCM to that in the homologous active site of *E. coli* CM (Figure 3). A significant difference between the two active sites is the interaction of the ether oxygen of the substrate with Gln88 in *E. coli* CM compared with Glu246 in YCM. Although both sidechains are capable of similar hydrogen-bonding interactions, only the glutamate sidechain might have a role as a general acid in the reversible protonation of the ether oxygen, a mechanistic possibility discussed previously in the absence of structural data [10]. Mutation of Glu246 to a glutamine resulted in an enzyme which had an around sevenfold reduced k_{cat} but also a higher substrate affinity such that k_{cat}/K_m of the mutant was similar to that of the activated wild-type enzyme [19]. In contrast to wild-type YCM, which has a narrow pH profile with optimum activity at pH 5.5, the Glu246→Gln mutant has activity between pH 4 and 10 with no well-defined optimum. On the other hand, the Gln88→Glu mutant of *E. coli* CM has kinetic properties which are similar to the activated yeast enzyme [24]. Thus, the conserved active sites of the two CMs and the similar properties of the glutamate/glutamine mutants indicate that both enzymes do not stabilize significantly different transition states. The fact that wild-type YCM and the Gln88→Glu mutant of *E. coli* CM have higher k_{cat} constants than the respective enzymes with a glutamine residue suggests that a better transition-state stabilization is achieved with a glutamate sidechain, possibly involving a transient protonation step, or repulsion of the leaving ether oxygen. This advantage is compensated by the lower substrate affinity of these enzymes and a restriction of the activity to acid pH.

In addition, a conjugation of the π-electrons of the two carboxylate groups of the substrate with the π-electrons of the chair-like transition state might reduce the activation energy. Both carboxylate groups of the inhibitor are approximately positioned for such an interaction by the two arginine sidechains (residues 16 and 157). However, due to the different hybridization of C1 and C8 (sp^3 in the inhibitor and sp^2 in the presumed transition state), the inhibitor is not a perfect transition-state analogue to study this interaction.

Structural studies on the three CMs of *B. subtilis*, yeast and *E. coli* as well as many biochemical studies indicate that these enzymes largely catalyze the pericyclic rearrangement by two ways. Firstly, binding of the active pseudodiaxial conformation of the substrate to the active site is achieved by polar interactions of the substrate's carboxylate and hydroxyl groups with the enzyme. This has been suggested previously following interpretation of an inverse secondary isotope effect at C4 of chorismate [10] and on the basis of the structure of *B. subtilis* CM [16]. Secondly, the transition state of the reaction is stabilized by hydrogen-bonding interactions between polar sidechains and the ether oxygen of the substrate. In all three enzymes, a positively charged residue might stabilize a developing negative charge on the ether oxygen. A development of negative charge on the ether oxygen occurs if the concerted rearrangement is asynchronous, such that breakage of the C–O bond is faster than formation of the C–C bond [25]. A role of electrostatic interactions in the stabilization of the transition state of the pericyclic reaction was proposed earlier for *B. subtilis* CM [13] and confirmed on the basis of the complex between the enzyme and the *endo*-oxabicyclic inhibitor [16].

Allosteric pathway

Tyrosine has polar contacts to both subunits, which contribute residues to a regulatory binding site; it forms hydrogen bonds with Arg75 and Arg76 of the 80s loop of

Figure 7

Interactions at the regulatory site in relation to the allosteric transition. Tyrosine (left) induces the T state by polar interactions to both sides of the dimer interface that bring H4/L80s and H8 closer together. Tryptophan (right) pushes the two monomers apart and causes a rotation of the two subunits to the R-state structure.

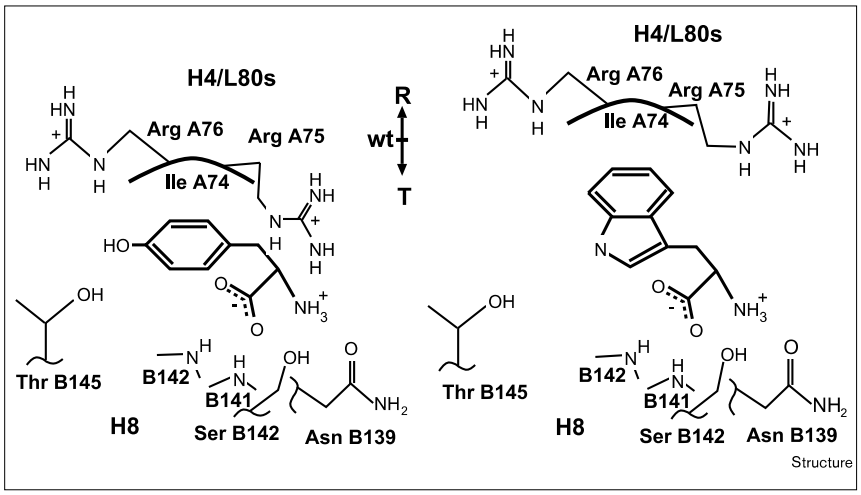

one monomer and to five residues of helix H8 of the other monomer (Figures 5 and 7). The phenolic OH group and the amino acid groups are involved in these interactions. These polar interactions are assumed to bring the regulatory domain and the catalytic domain of the neighboring monomer closer together than in the unliganded wild-type enzyme, for which no crystal structure is yet available, however. Tryptophan binds in a very similar way as tyrosine, such that the amino and carboxylate groups and the five-membered ring of the tryptophan sidechain are very close to the position of the amino and carboxylate groups and the phenolic sidechain of tyrosine, respectively (Figure 5c). Tryptophan, however, makes polar interactions through its amino acid groups only with residues of helix H8. The presence of the six-membered ring of tryptophan pushes the 80s loop and the regulatory domain away from helix H8. A major factor in the initiation of allosteric movements to the R state seems to be the steric interaction of the six-membered ring with the sidechain of Ile74. In contrast to interactions with tyrosine in the R state structure, Arg75 and Arg76 have no polar interactions with tryptophan, but van der Waals interactions might exist.

Binding of tryptophan causes a rotation of the two catalytic domains by 15° relative to their position in the tyrosine-bound T state. The allosteric rotation axis is perpendicular to the dimer axis (Figure 1). The regulatory domain does not follow this rotation. Instead, this domain moves in the other direction, away from the effector-binding site. As a result of the rotation of the two catalytic domains, many interactions at the dimer interface are rearranged. These changes at the dimer interface cause further movements within the catalytic domain that transmit the allosteric signal to the catalytic site.

Figures 8 and 9 show such a putative allosteric pathway from the dimer interface to the catalytic site. The conformational changes originate from the four residues Tyr212, Tyr212′, Phe28 and Phe28′, which interact with each other at the subunit–subunit interface. In the R-state structure (ITRP, white carbons in Figure 8), the sidechain of Tyr212 points towards the active site and interacts with Asp24 of H2, which in turn is hydrogen bonded to Lys208 of the neighboring helix H11. Glu23, the residue next to Asp24, interacts with Arg204 of H11. Arg157 is free to bind a carboxylate group of the substrate, as seen in the enzyme–inhibitor complex in ITRP (Figure 3); Glu23 is 6.6 Å away from the substrate's carboxylate group. In the T state, Tyr212 has a different sidechain conformation — Tyr212 and Tyr212′ move between the two phenylalanine residues (residues 28 and 28′) at the dimer interface. Thereby Phe28, which in the R state is closer to the dimer interface, is together with this part of helix H2 pushed toward the active site. As a result, Asp24 and Glu23 of helix H2 also move closer to the active site and change their partners for salt bridges — Asp24 now interacts with Arg204. The carboxylate group of Glu23, which was previously interacting with Arg204 in the R state, in turn moves by 5.0 Å into the active site to interact with Arg157 in the T state. If the inhibitor were present in this structure at the same position as in the R-state structure, the carboxylate group of Glu23 would be only 3.2 Å away from the substrate's carboxylate group. Thus, the conformation of Glu23 in the T-state structure probably strongly affects substrate binding. Moreover, Arg157 interacts with substrate less favorably and with less effective charge in the T state. Other active-site residues, including Lys168 and Glu246 shown in Figure 8, show only minor differences between T and R state structures. Although other residues at the dimer interface also have

Figure 8

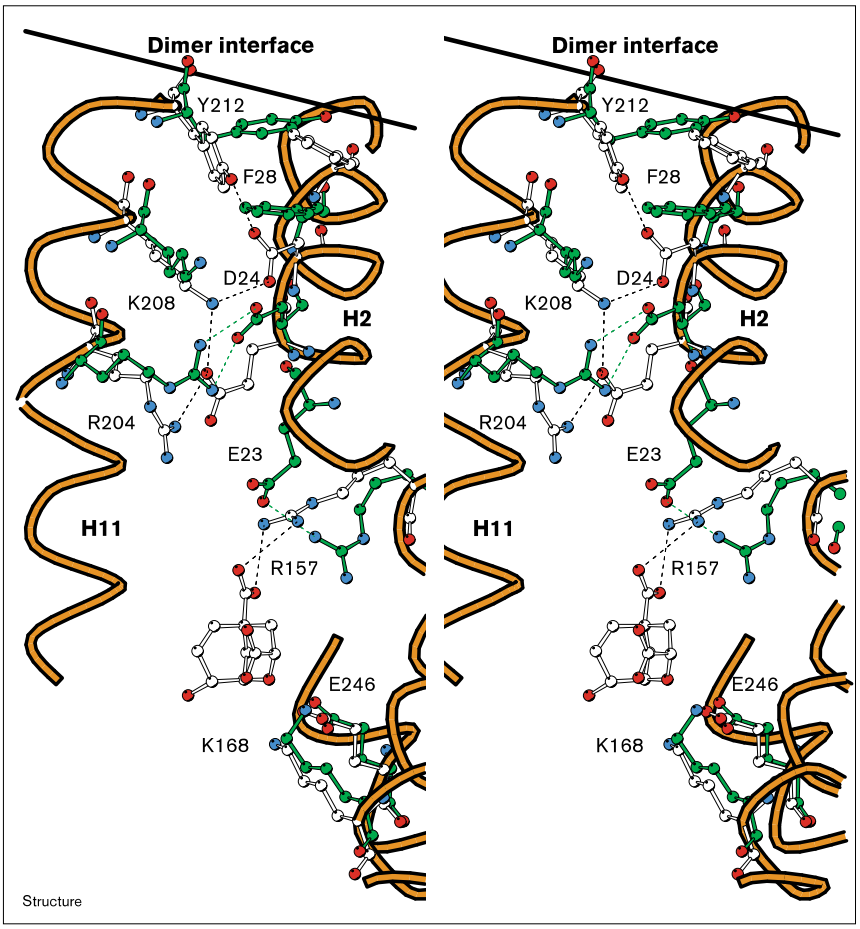

A proposed allosteric pathway between the dimer interface and the active site shown in stereo. Selected residues of ITRP (white carbons) and TYR (green) are superimposed. The two structures were superimposed based on residues of the catalytic domain of one monomer of the YCM dimer (see Materials and methods). The black line at the top of the figure marks the dimer axis in ITRP.

different conformations or interactions in the T and R state structures, there are no other examples in which these changes appear to be transmitted toward the active site, causing significant differences.

Figure 9

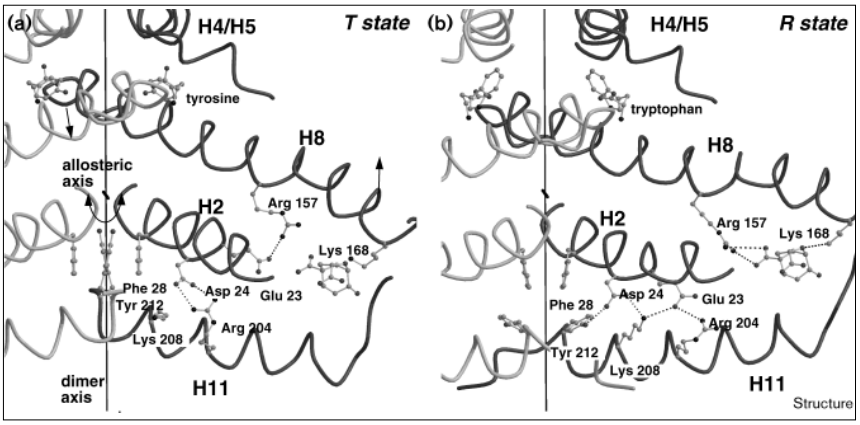

Conformational changes of Phe28 and Tyr212 between **(a)** T state (TYR) and **(b)** R state (ITRP) in relation to the allosteric pathway. The view is along the allosteric rotation axis perpendicular to the dimer axis (both axes are shown), similar to Figure 2. For reference, the *endo*-oxabicyclic inhibitor is shown in the T-state structure at a position derived from a superposition of the catalytic domain with ITRP.

The allosteric pathway we propose here does not include a direct connection between the regulatory site and the active site. Instead, binding of the effector causes a rotation of the monomers relative to each other, which is a typical feature of allosteric transitions of multimeric proteins. The long helix H8, which spans the whole monomer and extends from the regulatory site to the active site, probably serves as a lever by which tryptophan can initiate the rotation of the catalytic domain (Figure 9). This rotation causes conformational changes at the interface between the rotating monomers, which are then transmitted to the active site. Thus, the rotation of subunits serves as a means to transmit conformational changes from the regulatory site to any point at the subunit interface. The distance between the effector and Tyr212 is ~20 Å in YCM. The allosteric interaction between active sites (homotropic cooperative effect) could be transmit--ted along the same pathway, across the dimer interface. Tyr212 and Phe28 are at a special position at the dimer interface, because they are directly next to the dimer axis and all four residues (212, 212′, 28 and 28′) interact with each other between subunits. Interestingly, Tyr212 is also the first residue of the partially disordered 220s loop (residues 212–226), which probably has an important role in the allosteric transition (see above). The conformation of this loop might influence the conformation of Tyr212.

The X-ray structures of YCM in complex with the *endo*-oxabicyclic transition state analogue inhibitor showed the enzyme in a state in which the monomers are rotated relative to each other by about 22° with respect to the T state (0° rotation). The enzyme is present in this super R state even when the allosteric inhibitor tyrosine is bound to the regulatory site. Thus, it seems likely that this is the catalytically active state. Binding of tryptophan brings the enzyme, by a rotation angle of 15°, close to this active state, whereas the tyrosine-bound enzyme structure defines the T state (0° rotation, by definition). Binding of tryptophan activates YCM ~10-fold, whereas tyrosine inhibits the enzyme by about the same factor. Thus, the structure of the enzyme in the absence of effectors might be expected to have a rotation angle between 0° and 15°. Alternatively, the three states determined so far are the only stable minima along the transition from the T state to the active super R state, and the kinetics of the unliganded enzyme are a result of an equilibrium among these three different states.

In addition, the super R state structure of ITYR suggests that the T state structure as seen in TYR might show extremely low activity, but requires the transformation to the R state for effective catalytic turnover. The different kinetic behaviour (K_m is increased by a factor of 30 in the T state compared to the R state) is caused by a conformational change of the protein to the R state preceeding the catalytic step. The induction of R-state structures by both the allosteric activator as well as a transition-state analogue are in agreement with the heterotropic and homotropic allosteric behavior of the enzyme.

As the binding of relatively small ligands induces these conformational changes along the allosteric pathway, it might be expected that other forces, such as crystal-packing interactions, might especially influence the structures of allosteric proteins. Although this possibility cannot be excluded here as in other similar studies, the similarity of the R-state structures TRP and STRP, which were crystallized in different space groups, argues against this possibility.

Biological implications

Chorismate mutase (CM) catalyzes the conversion of chorismate to prephenate, the first committed step in the biosynthesis of the aromatic amino acids tyrosine and phenylalanine. The enzyme is allosterically regulated in two ways — feedback inhibition by tyrosine and activation by tryptophan. Tryptophan is the product of the other branch of the synthesis of aromatic amino acids, which begins with the conversion of chorismate to anthranilate by anthranilate synthase. As a relatively small allosteric protein, yeast chorismate mutase provides an ideal model system for exploring the detailed mechanisms of allosteric regulation. The reaction mechanism involving the Claisen rearrangement of chorismate to prephenate, notably the only known example of an enzyme-catalyzed pericyclic reaction, has also raised considerable interest in these enzymes. The design of inhibitors on the basis of structural information on chorismate mutases, which are present in archaebateria, eubacteria, plants, yeast and fungi, but not in humans and animals, has the potential for the development of new bacteriocides, herbicides and fungicides.

Our studies on the crystal structures of dimeric yeast CM in the inactive T and active R states and with a bound transition state analogue inhibitor define the structural changes between the two allosteric states and their influence on the active-site structure. Binding of the allosteric effectors to the regulatory-binding site at the dimer interface causes rotations of the catalytic domains, such that in the R state the monomers are rotated 15° relative to each other (where 0° rotation defines the T state). In the presence of the transition-state analogue, a super R state is formed, the monomer–monomer angle of which differs by 22° from the T state. The interactions between the effectors and residues at the regulatory site which cause these rotations in different directions are characterized. Tyrosine keeps the two subunits close together at a contact point between helix H8 and the 80s loop, by forming polar interactions with both these structural elements. Tryptophan pushes the subunits apart due to the larger size of its additional

six-membered ring. An allosteric pathway is proposed that links conformational changes at the dimer interface resulting from the rotation of subunits to changes in the active site, involving residues Tyr212, Phe28, Asp24, Glu23, Lys208 and Arg204.

Rotations of subunits are a typical feature of the allosteric transition of multimeric proteins by which conformational changes can be transmitted over long distances from the effector-binding site to any point at the subunit interface. The present study reveals structural insight into the function of such an allosteric pathway on a molecular level. This model for the mechanism of the allosteric transition is subject to further studies, especially those on suitable mutant enzymes. In addition, the detailed structural characterisation of the allosteric pathway forms the basis for a broader understanding of the mechanisms of allosteric regulation, for example by enabling an analysis by other means such as computational methods.

Binding of an *endo*-oxabicyclic transition state analogue inhibitor to yeast CM confirms the postulated binding mode, based on the distant relationship with *E. coli* chorismate mutase, and allows for an analysis of the interactions which stabilize the transition state of the catalytic reaction. Binding of the substrate as the pseudo-diaxial conformer, which is required for the pericyclic reaction, and transition-state stabilization by electrostatic interactions, particularly of the ether oxygen of the substrate which develops a partial negative charge in the course of a concerted but asynchronous reaction, are the main factors for the 10^6-fold rate enhancement by the wild-type enzymes over the uncatalyzed reaction.

Materials and methods

Crystallization and data collection

Wild-type and mutant YCM were isolated as described previously [3]. Crystals were grown by the hanging-drop method. For the R32 crystal form of ITRP, the protein solution was equilibrated against a solution of 19 % (w/v) polyethyleneglycol monomethylether 5000, 5 mM dithiothreitol, 0.15 M Tris HCl, pH 8.0, 0.15 M sodium acetate and 16 mM tryptophan. For ITYR, the reservoir contained 32% (w/v) polyethyleneglycol monomethylether 550, 4 mM dithiothreitol, 0.1 M Tris HCl, pH 9.0, 0.1 M sodium chloride and 2 mM tyrosine. The drops contained at the beginning of the vapor diffusion crystallization procedure approximately 10 mg/ml protein, 3 mM *endo*-oxabicyclic inhibitor and half of the reservoir buffer concentration. Rhombohedral crystals of size 0.3 × 0.3 × 0.3 mm^3 grew within about one week.

For the C2 crystal form of the Thr226→Ser mutant, the protein solution was equilibrated against a solution of 19% polyethylene glycol 3350, 3 mM dithiothreitol, 0.16 M sodium acetate, pH 5.0, and 16 mM tryptophan. The drop contained ~10 mg/ml protein and half of the concentration of the reservoir buffer. Plate-like crystals of size $0.8 \times 0.8 \times 0.2$ mm^3 appeared within one week.

Data for the two R32 crystal forms were collected at −150°C from crystals mounted in a hair-loop free-standing film of a cryo-buffer containing glycerol. The crystals were transferred stepwise to solutions containing increasing amounts of glycerol in the reservoir buffer until a final concentration of 20% (v/v) glycerol was reached. X-ray diffraction data for the C2 crystals were collected in a sealed capillary at room temperature. Table 3 summarizes the details of data collection on a Siemens (Madison, WI) model X-1000 multiwire area detector and of data reduction with the program XDS [26].

Structure determination and refinement

The three structures were solved by molecular replacement (program AMORE [27]) using the model for YCM in the R state as the search model. Crystallographic refinement was performed using X-PLOR [28] by several rounds of manual rebuilding (program O [29]), simulated annealing and positional minimization. The R32 crystal form contains two independent monomers in the asymmetric unit which belong to different protein dimers. For ITRP at 3.0 Å resolution, strict non-crystallographic symmetry restraints were employed. Refinement of the two monomers independently with energy-based restraints yielded higher R_{free} values after refinement. For ITYR, however, independent refinement of the two monomers with ncs-restraints resulted in better R values. Restraints were employed on the mainchain and sidechains atoms except for those involved in crystal contacts. STRP contains one subunit in the asymmetric unit. 85 water molecules were included manually from $|F_o - F_c|$ difference electron maps for STRP.

The exogenous ligands were introduced into the model, when the protein model was already well refined and the density of the effectors and the inhibitor was clear. For all ligands there was strong density present at the corresponding binding sites which could be readily interpreted. For ITRP the *endo*-oxabicyclic inhibitor was refined to relatively high B values which are usually only observed for disordered residues (Table 3). The electron density maps, even before the inhibitor was introduced into the model, were well defined and clearly demonstrated binding of this inhibitor, however. The high B values could be a result of some positional disorder of the ligand, possibly also between the two subunits which, because of the limited resolution, were not refined independently. Other causes might be a partial occupancy of the ligand or an artifact resulting from the relatively low resolution data.

In addition to those programs mentioned above, programs of the CCP4 suite [30] were used for the crystallographic analysis. All non-schematic figures were calculated using program BOBSCRIPT (R Esnouf, Leuven, Belgium), which is derived from program MOLSCRIPT [31].

Superpositions

The matrices for a superposition of different models or regions were calculated by a least-squares distance minimization algorithm implemented inside the program O [29] using Cα atoms. For the superposition of the whole monomer or dimer of different YCM models residues 1–214 and 224–256 were used. Residues 6–43, 108–211, and 231–251 were used for the alignment of the catalytic domains. The dimer of *E. coli* CM was superimposed onto a YCM monomer using residues 13–27, 146–171, 192–211, and 238–252 of YCM and B8–B22, A17–A42, A46–A65, and A80–A94 of *E. coli* CM.

Accession numbers

Structure coordinates were deposited with the Brookhaven Protein Data Bank with the codes 3csm, 4csm and 5csm for the ITRP, ITYR and STRP structures, respectively.

Note added in proof

A very recent molecular dynamics study of docking of the *endo*-oxabicyclic transition-state analogue to the YCM molecule finds that Glu246 is hydrogen bonded to the ether oxygen via a water bridge, rather than directly (Lin, S.L., Xu, D., Li, A., Rosen, M., Wolfson, H.J. & Nussinov, R. (1997). Investigation of the enzymatic mechanism of the yeast chorismate mutase by docking a transition state analog. *J. Mol. Biol.* **271**, 838–845). The refined structures ITRP and ITYR of the present study, however, show the Glu246 sidechain in close distance to the ether oxygen.

Table 3

Details of data collection and refinement.

	ITRP	ITYR	STRP
Data set statistics			
Space group	R32	R32	C2
Cell axes (Å)	a = 203.5, c = 128.7	a = 205.5, c = 131.2	a = 94.6, b = 51.4, c = 66.8, β = 116.6°
Maximum resolution (Å)	3.0	2.8	2.0
Number of crystals	1	1	1
Temperature (°C)	−150	−150	20
Reflections measured	51,388	64,883	40,918
Unique reflections	20,253	25,765	18,951
Completeness (%)*	98.4 (99.1)	98.2 (97.8)	96.6 (88.8)
Completeness >1σI (%)*	83.0 (65.4)	86.0 (70.0)	89.2 (68.7)
R_{sym}*	0.092 (0.325)	0.084 (0.291)	0.055 (0.196)
Vm (Å³/Da)	4.3	4.5	2.4
Refinement statistics			
Resolution range (Å)*	15.0–3.0 (3.2–3.0)	15.0–2.8 (2.9–2.8)	7.0–2.0 (2.1–2.0)
R / R_{free}†	0.204 / 0.247	0.213 / 0.270	0.186 / 0.236
Rmsd			
bond length (Å)	0.013	0.012	0.012
bond angles (°)	2.0	1.9	1.9
dihedral angles (°)	19.0	18.6	19.7
improper twist angles (°)	1.7	1.6	1.6
Average B factor			
protein (Å²)	38.4	40.6	26.3
effector (Å²)	17.4	31.7	14.9
inhibitor (Å²)	88.3	36.5	–
waters (Å²)	–	–	38.4
Ramachandran plot			
outliers (%)	0	0	0
most favoured regions (%)	88.0	86.9	92.4

*These values in parentheses are for the highest resolution shell. †8% of the reflections were used to calculate R_{free}.

Acknowledgements

We thank PA Bartlett for the gift of the *endo*-oxabicyclic inhibitor. This work was supported by grants from the National Institutes of Health (GM 06920 to WNL) and from the Deutsche Forschungsgemeinschaft (BR1502 to GB). NS thanks the Deutsche Forschungsgemeinschaft for financial support and W Saenger for support in his laboratory.

References

1. Weiss, U. & Edwards, J.M. (1980). The biosynthesis of aromatic amino compounds. Wiley, New York, USA.
2. Braus, G.H. (1991). Aromatic amino acid biosynthesis in the yeast *Saccharomyces cerevisiae*: a model system for the regulation of a eukaryotic biosynthetic pathway. *Microbiol. Rev.* **55**, 349–370.
3. Schmidheini, T., Mösch, H.-U., Evans, J.N. & Braus, G. (1990). Yeast allosteric chorismate mutase is locked in the activated state by a single amino acid substitution. *Biochemistry* **29**, 3660–3668.
4. Xue, Y., Lipscomb, W.N., Gray, R., Schnappauf, G. & Braus, G. (1994). The crystal structure of allosteric chorismate mutase at 2.2-Å resolution. *Proc. Natl. Acad. Sci. USA* **91**, 10814–10818.
5. Sträter, N., Håkansson, K., Schnappauf, G., Braus, G. & Lipscomb, W.N. (1996). Crystal structure of the T state of allosteric yeast chorismate mutase and comparison with the R state. *Proc. Natl. Acad. Sci. USA* **93**, 3330–3334.
6. Ganem, B. (1996). The mechanism of the Claisen rearrangement: déjà vu all over again. *Angew. Chem. Int. Ed. Engl.* **35**, 936–945.
7. Andrews, P.R., Smith, G.D. & Young, I.G. (1973). Transition state stabilization and enzymic catalysis. Kinetic and molecular orbital studies of the rearrangement of chorismate to prephenate. *Biochemistry* **12**, 3492–3498.
8. Sogo, S.G., Widlanski, T.S., Hoare, J.H., Grimshaw, C.E., Berchtold, G.A. & Knowles, J.R. (1984). Stereochemistry of the rearrangement of chorismate to prephenate: chorismate mutase involves a chair transition state. *J. Am. Chem. Soc.* **106**, 2701–2703.

9. Addadi, L., Jaffee, E.K. & Knowles, J.R. (1983). Secondary tritium isotope effects as probes of the enzymic and nonenzymic conversion of chorismate to prephenate. *Biochemistry* **22**, 4494–4501.
10. Guilford, W.J., Copley, S.D. & Knowles, J.R. (1987). On the mechanism of the chorismate mutase reaction. *J. Am. Chem. Soc.* **109**, 5013–5019.
11. Copley, S.D. & Knowles, J.R. (1987). The conformational equilibrium of chorismate in solution: implications for the mechanism of the non-enzymic and the enzyme-catalyzed rearrangement of chorismate to prephenate. *J. Am. Chem. Soc.* **109**, 5008–5013.
12. Görisch, H. (1978). On the mechanism of the chorismate mutase reaction. *Biochemistry* **17**, 3700–3705.
13. Gray, J.V. & Knowles J.R. (1994). Monofunctional chorismate mutase from *Bacillus subtilis*: FTIR studies and the mechanism of action of the enzyme. *Biochemistry* **33**, 9953–9959.
14. Bartlett, P.A. & Johnson, C.R. (1985). An inhibitor of chorismate mutase resembling the transition-state conformation. *J. Am. Chem. Soc.* **107**, 7792–7793.
15. Chook, Y.M., Ke, H. & Lipscomb, W.N. (1993). Crystal structures of the monofunctional chorismate mutase from *Bacillus subtilis* and its complex with a transition state analog. *Proc. Natl. Acad. Sci. USA* **90**, 8600–8603.
16. Chook, Y.M., Gray, J.V., Ke, H. & Lipscomb, W.N. (1994). The monofunctional chorismate mutase from *Bacillus subtilis*. Structure determination of chorismate mutase and its complexes with a transition state analog and prephenate, and implications for the mechanism of the enzymatic reaction. *J. Mol. Biol.* **240**, 476–500.
17. Lee, A.Y., Karplus, P.A., Ganem, B. & Clardy, J. (1995). Atomic structure of the buried catalytic pocket of *Escherichia coli* chorismate mutase. *J. Am. Chem. Soc.* **117**, 3627–3628.
18. Xue, Y. & Lipscomb, W.N. (1995). Location of the active site of allosteric chorismate mutase from *Saccharomyces cerevisiae*, and comments on the catalytic and regulatory mechanisms. *Proc. Natl. Acad. Sci. USA* **92**, 10595–10598.
19. Schnappauf, G., Sträter, N., Lipscomb, W.N. & Braus, G.H. (1997). A glutamate residue in the catalytic center of the yeast chorismate mutase restricts enzyme activity to acidic conditions. *Proc. Natl. Acad. Sci. USA* **94**, 8491–8496.
20. Haynes, M.R., Stura, E.A., Hilvert, D. & Wilson, I.A. (1994). Routes to catalysis: structure of a catalytic antibody and comparison with its natural counterpart. *Science* **263**, 646–652.
21. Jackson, D.Y., Liang, M.N., Bartlett, P.A. & Schultz, P.G. (1992). Activation parameters and stereochemistry of an antibody-catalyzed Claisen rearrangement. *Angew. Chem. Int. Ed. Engl.* **31**, 182–183.
22. Lee, A.Y., Stewart, J.D., Clardy, J. & Ganem, B. (1995). New insight into the catalytic mechanism of chorismate mutase from structural studies. *Chem. Biol.* **2**, 195–203.
23. Graf, R., Dubaquié, Y. & Braus, G.H. (1995). Modulation of the allosteric equilibrium of yeast chorismate mutase by variation of a single amino acid residue. *J. Bacteriol.* **177**, 1645–1648.
24. Galopin, C.C., Zhang, S., Wilson, D.B. & Ganem, B. (1996). On the mechanism of chorismate mutases: clues from wild-type *E. coli* enzyme and a site-directed mutant related to yeast chorismate mutase. *Tetrahedron Lett.* **37**, 8675–8678.
25. Gajewski, J.J. (1980). Energy surfaces of sigmatropic shifts. *Acc. Chem. Res.* **13**, 142–148.
26. Kabsch, W. (1988). Evaluation of single crystal X-ray diffraction data from a position-sensitive detector. *J. Appl. Cryst.* **21**, 916–924.
27. Navaza, J. (1994). AMoRe: an automated package for molecular replacement. *Acta Cryst. A* **50**, 157–163.
28. Brünger, A.T. (1992). *X-PLOR, Manual Version 3.1*. Yale University Press, New Haven, CT, USA.
29. Jones, A.T. & Kjeldgaard, M. (1993). *O: the manual. Version 5.9.* Uppsala, Sweden.
30. CCP4 (1994). The CCP4 suite: programs for protein crystallography. *Acta Cryst. D* **50**, 760–763.
31. Kraulis, P.J. (1991). MOLSCRIPT: a program to produce both detailed and schematic plots of protein structures. *J. Appl. Cryst.* **24**, 946–950.